

Single broadband source depth estimation using Stokes parameters in shallow water

Yizheng Wei(韦宜政), Chao Sun(孙超), Lei Xie(谢磊), and Mingyang Li(李明杨)

Citation: Chin. Phys. B, 2026, 35 (**2**): 024301. DOI: 10.1088/1674-1056/adee01
http://cpb.iphy.ac.cn; http://iopscience.iop.org/cpb

What follows is a list of articles you may be interested in

Three-dimensional acoustic propagation model for shallow waters based on an indirect boundary element method

Edmundo F. Lavia, Juan D. Gonzalez, and Silvia Blanc
Chin. Phys. B, 2023, 32 (**5**): 054301. DOI: 10.1088/1674-1056/ac90b1

Effect of bio-tissue deformation behavior due to intratumoral injection on magnetic hyperthermia

Yundong Tang(汤云东), Jian Zou(邹建), Rodolfo C.C. Flesch, and Tao Jin(金涛)
Chin. Phys. B, 2023, 32 (**3**): 034304. DOI: 10.1088/1674-1056/ac744c

A passive source ranging method based on the frequency warping transform of the vertical intensity flux in shallow water

Yu-Bo Qi(戚聿波), Shi-Hong Zhou(周士弘), Meng-Xiao Yu(于梦枭), Shu-Yuan Du(杜淑媛), Mei Sun(孙梅), Ren-He Zhang(张仁和)
Chin. Phys. B, 2019, 28 (**5**): 054302. DOI: 10.1088/1674-1056/28/5/054302

Effects of rough surface on sound propagation in shallow water

Ruo-Yun Liu(刘若芸), Zheng-Lin Li(李整林)
Chin. Phys. B, 2019, 28 (**1**): 014302. DOI: 10.1088/1674-1056/28/1/014302

Bubble nonlinear dynamics and stimulated scattering process

Jie Shi(时洁), De-Sen Yang(杨德森), Sheng-Guo Shi(时胜国), Bo Hu(胡博), Hao-Yang Zhang(张昊阳), Shi-Yong Hu(胡诗涌)
Chin. Phys. B, 2016, 25 (**2**): 024304. DOI: 10.1088/1674-1056/25/2/024304

Single broadband source depth estimation using Stokes parameters in shallow water

Yizheng Wei(韦宜政)[1,2], Chao Sun(孙超)[1,2], Lei Xie(谢磊)[1,2,†], and Mingyang Li(李明杨)[1,2,‡]

[1] *School of Marine Science and Technology, Northwestern Polytechnical University, Xi'an* 710072, *China*
[2] *Key Laboratory of Ocean Acoustic and Sensing, Ministry of Industry and Information Technology, Northwestern Polytechnical University, Xi'an* 710072, *China*

(Received 17 March 2025; revised manuscript received 7 July 2025; accepted manuscript online 10 July 2025)

Presented in this study is a novel method for estimating the depth of single underwater source in shallow water, utilizing vector sensors. The approach leverages the depth distribution of the broadband Stokes parameters to estimate source depth accurately. Unlike traditional matched field processing (MFP) and matched mode processing (MMP), the proposed approach can estimate source depth directly from the data received by sensors without requiring complete environmental information. Firstly, the broadband Stokes parameters (BSP) are established using the normal mode theory. Then the nonstationary phase approximation is used to simplify the theoretical derivation, which is necessary when dealing with broadband integrals. Additionally, range terms of the BSP are eliminated by normalization. By analyzing the depth distribution of the normalized broadband Stokes parameters (NBSP), it is found that the NBSP exhibit extreme values at the source depth, which can be used for source depth estimation. So the proposed depth estimation method is based on searching the peaks of the NBSP. Simulations show that this method is effective in relatively simple shallow water environments. Finally, the effect of source range, frequency bandwidth, sound speed profile (SSP), water depth, and signal-to-noise ratio (SNR) are studied. The findings indicate that the proposed method can accurately estimate the source depth when the SNR is greater than -5 dB and does not need to consider model mismatch issues. Additionally, variations in environmental parameters have minimal impact on estimation accuracy. Compared to MFP, the proposed method requires a higher SNR, but demonstrates superior robustness against fluctuations in environmental parameters.

Keywords: broadband source depth estimation, shallow water, polarization, Stokes parameters

PACS: 43.30.+m, 43.60.Jn, 43.60.–c, 43.30.Bp

DOI: 10.1088/1674-1056/adee01 **CSTR:** 32038.14.CPB.adee01

1. Introduction

Source depth estimation is a significant issue in underwater target localization. For the study of source depth estimation, matched field processing (MFP) and matched mode processing (MMP) are the most widely used methods. In MFP, the received data are matched with the replica field using a model of underwater acoustic propagation to determine source location.[1,2] However, calculating the replica field requires complete knowledge of environmental parameters, and mismatches in these parameters significantly affect the estimation results. In contrast, MMP estimates the source position by matching the mode amplitudes calculated from pressure data, which enhances its robustness against environmental mismatches.[3,4] But MMP methods typically require the horizontal aperture. In response to the challenge of limited horizontal aperture, researchers have developed a number of methods for estimating the depth of moving sources based on the horizontal synthetic aperture generated by the source motion.[5,6] In addition, some methods based on multipath arrival structure[7,8] and interference structure[9,10] have been proposed to improve the estimation accuracy and robustness. In this work, a broadband source depth estimation method based on polarization in shallow water is proposed, without requiring any environmental information or source is moving.

Polarization is a characteristic of vector signals that describes the path of the vector endpoint as it moves over time at a fixed location. Shchurov[11] found that when two plane waves with identical frequency but different phases interfere, the resultant vector of the particle velocity is a rotating vector and the path of the endpoint of the vector is an ellipse. He refers to this as polarization in the acoustic field. Shi[12] conducted experiments which showed that the rotation of the particle velocity vector occurs when two plane waves interfere, offering proof of the presence of polarization in the acoustic field.

Since the polarization of sound field is related to the particle velocity, it is necessary to use vector sensor to measure it. Considering that polarization may bring more information to vector sensor acoustic signal processing, researchers specializing in underwater acoustics proposed some frameworks for describing acoustic field polarization. Dall'Osto and Dahl[13] found that the interference of sound waves through multiple paths in shallow water waveguides results in the elliptical particle movements and suggested employing circularity to char-

†Corresponding author. E-mail: xielei2014@mail.nwpu.edu.cn
‡Corresponding author. E-mail: mingyang.li@nwpu.edu.cn

© 2026 Chinese Physical Society and IOP Publishing Ltd. All rights, including for text and data mining, AI training, and similar technologies, are reserved.

acterize the rotation of the particle. Subsequently, they applied circularity to geoacoustic inversion.[14,15] Bonnel *et al.*,[16] combining the Stokes parameters with normal mode theory, proposed a framework of Stokes parameters for describing the polarization in the underwater acoustic field. And then Dahl *et al.*[17] highlighted the potential use of the Stokes parameters in localizing sources. Chen *et al.*[18] proposed a conventional beamforming (CBF) algorithm combined with polarization filtering to enhance the signal-to-noise ratio of the CBF algorithm, which is based on the framework of Stokes parameters.

It can be observed that the Stokes parameters framework holds both research and application value in the field of underwater acoustics. So in this paper, we choose the Stokes parameters framework to estimate the source depth. Firstly, the broadband Stokes parameters (BSP) are proposed for the broadband source.[19] Then we use the nonstationary phase approximation to simplify the analysis.[20] Although both this paper and reference[20] utilize the nonstationary phase approximation, there is a clear distinction between the two studies in terms of their research focus. The authors in Ref. [20] investigated the difference between potential energy and kinetic energy in a sound field, whereas this paper focuses on polarization characteristics, specifically the Stokes parameters. These two studies differ not only in their physical interpretations but also in their depth-dependent properties (e.g., S_3). Subsequently, we can obtain the normalized broadband Stokes parameters by normalization, which are independent on range and solely dependent on the source depth as well as the environment. At the source depth, the normalized broadband Stokes parameters undergo significant changes, which can be used for depth estimation. Finally, the depth estimation results are obtained by searching the peak of the normalized broadband Stokes parameters. Note that the proposed method directly estimates the source depth from the received data without the need for environmental information to calculate the replica field, and the depths of the receivers will affect the estimation performance.

The subsequent sections of this paper are arranged as follows. Section 2 introduces the principal theory of polarization for broadband source in shallow water. And the depth estimation method is shown in Section 3. Section 4 conducts a numerical simulation. Section 5 offers a conclusion for the study.

2. Polarization of sound field

2.1. The broadband Stokes parameters

In the sound field, the Stokes parameters can be expressed by the particle velocity as[16]

$$\begin{aligned} S_0(f) &= |v_r(f)|^2 + |v_z(f)|^2, \\ S_1(f) &= |v_r(f)|^2 - |v_z(f)|^2, \\ S_2(f) &= 2\mathrm{Re}\left[v_r(f)v_z^*(f)\right], \\ S_3(f) &= 2\mathrm{Im}\left[v_r(f)v_z^*(f)\right], \end{aligned} \tag{1}$$

where v_r and v_z are the horizontal and vertical particle velocities, respectively. S_0 represents pure energetic information while geometric polarization properties are provided by S_1, S_2, and S_3. Defining normalized Stokes parameters allows for the elimination of intensity dependence in S_1, S_2, S_3:

$$s_1(f) = \frac{S_1(f)}{S_0(f)}, \quad s_2(f) = \frac{S_2(f)}{S_0(f)}, \quad s_3(f) = \frac{S_3(f)}{S_0(f)}. \tag{2}$$

On the basis of the normal mode theory, when the source depth is z_s, the receiver depth is z, and the range between source and receiver is r, the received particle velocities in a range-independent waveguide, can be represented as

$$\begin{aligned} v_r(r,z,f) &= \Omega(f)\frac{\mathrm{i}\,\mathrm{e}^{-\mathrm{i}\pi/4}}{\rho^2(z_s)\omega\sqrt{8\pi r}} \\ &\quad \times \sum_{n=1}^{N} \varphi_n(z_s)\varphi_n(z)\sqrt{k_{rn}}\,\mathrm{e}^{\mathrm{i}k_{rn}r}, \end{aligned} \tag{3}$$

$$v_z(r,z,f) = \Omega(f)\frac{\mathrm{e}^{-\mathrm{i}\frac{\pi}{4}}}{\rho^2(z_s)\omega\sqrt{8\pi r}} \sum_{n=1}^{N} \varphi_n(z_s)\varphi_n'(z)\frac{\mathrm{e}^{\mathrm{i}k_{rn}r}}{\sqrt{k_{rn}}}, \tag{4}$$

where f represents the frequency, $\Omega(f)$ denotes the source spectrum, N stands for the number of propagating modes, $\rho(z_s)$ is the density of water at the source depth, φ_n and k_{rn} denote the eigenfunction and the horizontal wavenumber of the n-th mode, respectively. $\varphi'_n(z) = \partial\varphi_n(z)/\partial z$ is the partial derivative of $\varphi_n(z)$ with respect to z.

Substituting Eqs. (3) and (4) into Eq. (1), the Stokes parameters become

$$\begin{aligned} S_0(r,z,f) &= |v_r(r,z,f)|^2 + |v_z(r,z,f)|^2 = \frac{|Q(f)|^2}{r}\left\{\sum_{n=1}^{N}\varphi_n^2(z_s,f)\left[\varphi_n^2(z,f)k_{rn}(f) + \frac{\varphi'^2_n(z,f)}{k_{rn}(f)}\right]\right. \\ &\quad + \sum_{\substack{n,m=1\\ n\neq m}}^{N}\varphi_n(z_s,f)\varphi_m(z_s,f)\varphi_n(z,f)\varphi_m(z,f)\sqrt{k_{rn}(f)k_{rm}(f)}\,\mathrm{e}^{\mathrm{i}\Delta k_{nm}(f)r} \\ &\quad \left. + \sum_{\substack{n,m=1\\ n\neq m}}^{N}\varphi_n(z_s,f)\varphi_m(z_s,f)\varphi'_n(z,f)\varphi'_m(z,f)\frac{\mathrm{e}^{\mathrm{i}\Delta k_{nm}(f)r}}{\sqrt{k_{rn}(f)k_{rm}(f)}}\right\} \\ &= \sum_{n=1}^{N} I_{0,n}(r,z,f) + \sum_{\substack{n,m=1\\ n\neq m}}^{N} J_{0,nm}(r,z,f), \end{aligned} \tag{5a}$$

$$S_1(r,z,f) = |v_r(r,z,f)|^2 - |v_z(r,z,f)|^2 = \frac{|Q(f)|^2}{r}\left\{\sum_{n=1}^{N}\varphi_n^2(z_s,f)\left[\varphi_n^2(z,f)\,k_{rn}(f) - \frac{\varphi'^2_n(z,f)}{k_{rn}(f)}\right]\right.$$
$$+\sum_{\substack{n,m=1\\n\neq m}}^{N}\varphi_n(z_s,f)\,\varphi_m(z_s,f)\varphi_n(z,f)\,\varphi_m(z,f)\sqrt{k_{rn}(f)\,k_{rm}(f)}\,e^{i\Delta k_{nm}(f)r}$$
$$\left.-\sum_{\substack{n,m=1\\n\neq m}}^{N}\varphi_n(z_s,f)\,\varphi_m(z_s,f)\varphi'_n(z,f)\,\varphi'_m(z,f)\frac{e^{i\Delta k_{nm}(f)r}}{\sqrt{k_{rn}(f)\,k_{rm}(f)}}\right\} = \sum_{n=1}^{N}I_{1,n}(r,z,f) + \sum_{\substack{n,m=1\\n\neq m}}^{N}J_{1,nm}(r,z,f), \tag{5b}$$

$$S_2(r,z,f) = 2\cdot\mathrm{Re}\left[v_r(r,z,f)v_z^*(r,z,f)\right] = 2\frac{|Q(f)|^2}{r}\sum_{\substack{n,m=1\\n\neq m}}^{N}\varphi_n(z_s,f)\,\varphi_m(z_s,f)$$
$$\times\varphi_n(z,f)\,\varphi'_m(z,f)\sqrt{\frac{k_{rn}(f)}{k_{rm}(f)}}\sin(\Delta k_{nm}(f)\,r) = \sum_{\substack{n,m=1\\n\neq m}}^{N}J_{2,nm}(r,z,f), \tag{5c}$$

$$S_3(r,z,f) = 2\cdot\mathrm{Im}\left[v_r(r,z,f)v_z^*(r,z,f)\right] = 2\frac{|Q(f)|^2}{r}\left[\sum_{n}^{N}\varphi_n^2(z_s,f)\varphi_n(z,f)\,\varphi'_n(z,f)\right.$$
$$\left.+\sum_{\substack{n,m=1\\n\neq m}}^{N}\varphi_n(z_s,f)\,\varphi_m(z_s,f)\varphi_n(z,f)\,\varphi'_m(z,f)\sqrt{\frac{k_{rn}(f)}{k_{rm}(f)}}\cos(\Delta k_{nm}(f)\,r)\right]$$
$$= \sum_{n=1}^{N}I_{3,n}(r,z,f) + \sum_{\substack{n,m=1\\n\neq m}}^{N}J_{3,nm}(r,z,f), \tag{5d}$$

where $Q(f) = \Omega(f)e^{-i\pi/4}\rho^2(z_s)\omega\sqrt{8\pi}$, $\sum_{n=1}^{N}I_{k,n}$ $(k = 0,1,2,3,)$ and $\sum_{\substack{n,m=1\\n\neq m}}^{N}J_{k,nm}$ $(k = 0,1,2,3)$ represent the incoherent sum of each mode and the sum of coherent terms between modes, respectively.

For a broadband signal with a frequency band of $[f_1,f_2]$, we integrate the Stokes parameters over the bandwidth and define this integrated form as the broadband Stokes parameters (BSP)

$$S_k^{[f_1,f_2]}(r,z) \triangleq \int_{f_1}^{f_2}S_k(r,f,z)\,\mathrm{d}f = \sum_{n=1}^{N}I_{k,n}^{[f_1,f_2]}(r,z) + \sum_{\substack{n,m=1\\n\neq m}}^{N}J_{k,nm}^{[f_1,f_2]}(r,z). \tag{6}$$

As shown in Eq. (6), the BSP can be expressed as the sum of two terms: the incoherent terms $\sum_{n=1}^{N}I_{k,n}^{[f_1,f_2]}(r,z)$ and the cross-terms $\sum_{\substack{n,m=1\\n\neq m}}^{N}J_{k,nm}^{[f_1,f_2]}(r,z)$. The cross-terms are complicated, so we use the nonstationary phase approximation to simplify the analysis. According to Ref. [20], if the following two conditions are satisfied:

(i) the signal bandwidth is limited;

(ii) in the considered frequency band, the group velocities of any two distinct modes do not intersect, meaning that for all $m \neq n$, $\frac{\mathrm{d}k_m}{\mathrm{d}f} \neq \frac{\mathrm{d}k_n}{\mathrm{d}f}$. Although mode crossings may occasionally occur, such as in the vicinity of the Airy phase, the corresponding acoustic energy associated with these crossings is typically negligible. This condition is generally satisfied in relatively simple shallow water waveguide environments.

then $J_{k,nm}^{[f_1,f_2]}(z) \to 0$ as $r \to \infty$. These assumptions also represent the limitations of the proposed method in this paper.

When r is significantly larger than 1, an approximation for the BSP can be written as

$$S_0^{[f_1,f_2]}(r,z) \approx \sum_{n=1}^{N}I_{0,n}^{[f_1,f_2]}(r,z), \tag{7a}$$
$$S_1^{[f_1,f_2]}(r,z) \approx \sum_{n=1}^{N}I_{1,n}^{[f_1,f_2]}(r,z), \tag{7b}$$
$$S_2^{[f_1,f_2]}(r,z) \approx 0, \tag{7c}$$
$$S_3^{[f_1,f_2]}(r,z) \approx \sum_{n=1}^{N}I_{3,n}^{[f_1,f_2]}(r,z). \tag{7d}$$

As shown in Eq. (7c), $S_2^{[f_1,f_2]}(r,z) \approx 0$, so we do not analyze $S_2^{[f_1,f_2]}(z)$ later in the article. And the other three Stokes parameters are functions related to depth, their depth distribution characteristics are discussed in Subsection 2.2 below.

2.2. Depth distribution of the broadband Stokes parameters

In our previous work,[19] we analyzed the properties of the BSP for the ideal isovelocity shallow water waveguide, which is necessary to introduce in this section. After theoretical analysis, we also simulated the variation of the BSP with depth in an ideal waveguide, as shown in Fig. 1. The ideal isovelocity waveguide has a pressure release sea-surface and a rigid seafloor. In water column, the sound speed is 1500 m/s, the density is 1000 kg/m^3, and the depth is 100 m. The source depth is 25 m, the range is 5 km, and the integrated frequency band is $[10,250]$ Hz.

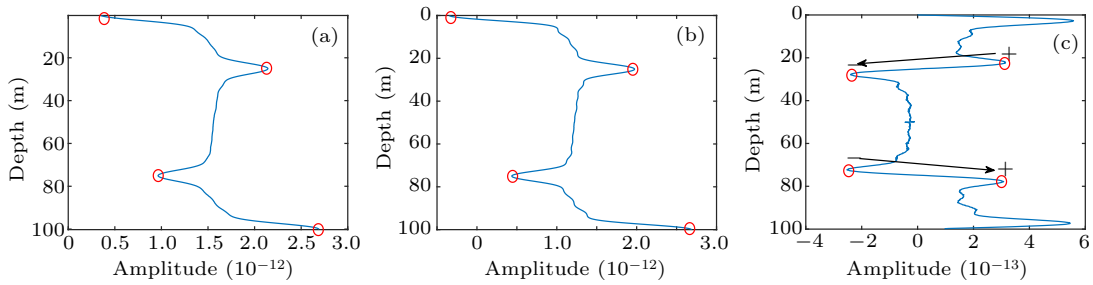


Fig. 1. Evolution of the BSP in an ideal isovelocity waveguide: (a) $S_0^{[10,250]}$, (b) $S_1^{[10,250]}$, (c) $S_3^{[10,250]}$.

According to Ref. [21], $\varphi_n(z)$ and k_{zn} in the ideal isovelocity shallow water waveguide can be expressed as

$$\varphi_n(z)=\sqrt{\frac{2\rho_0}{D}}\sin k_{zn}z,\quad k_{zn}=\frac{\pi}{D}\left(n-\frac{1}{2}\right). \tag{8}$$

Firstly, the S_0 is analyzed. Substituting Eq. (8) into Eq. (7a) gives the expression of $S_0^{[f_1,f_2]}(r,z)$

$$\begin{aligned}S_0^{[f_1,f_2]}(r,z)&\approx\sum_{n=1}^{N}I_{0,n}^{[f_1,f_2]}(r,z)\\&=\frac{1}{r}\left[\frac{1}{4}\left(\sum_{n=1}^{N}a_n^{[f_1,f_2]}-\varepsilon_0(z_s)-\varepsilon_0(z)\right.\right.\\&\quad\left.\left.+\frac{\varepsilon_0(z-z_s)+\varepsilon_0(z+z_s)}{2}\right)+G\right],\end{aligned} \tag{9}$$

where

$$\begin{aligned}&\varepsilon_0(z)=\sum_{n=1}^{N}a_n^{[f_1,f_2]}\cos(2k_{zn}z),\quad G=\sum_{n=1}^{N}g_n,\\&a_n^{[f_1,f_2]}=\int_{f_1}^{f_2}\frac{|Q(f)|^2}{k_{rn}(f)}\frac{4\rho_0^2}{D^2}\left(\frac{\omega^2}{c^2}-2k_{zn}^2\right)\mathrm{d}f,\\&g_n=\int_{f_1}^{f_2}\frac{|Q(f)|^2}{k_{rn}(f)}\frac{4\rho_0^2}{D^2}k_{zn}^2\mathrm{d}f.\end{aligned}$$

From Eq. (9), we can see that the depth characteristic of S_0 only depends on $\varepsilon_0(z)$. According to Ref. [20], $\varepsilon_0(z)$ can be expressed in the form of a convolution between a Dirichlet-like kernel, denoted as $D_N(z)$, and a smoothing operator $A(z)$

$$\varepsilon_0(z)=A(z)*D_N(z), \tag{10}$$

where $*$ represents the convolution operation. The depth dependence of $\varepsilon_0(z)$ is mainly related to $D_N(z)$

$$D_N(z)=\sum_{n=1}^{N}\cos(2k_{zn}z)=\cos\left(\frac{\pi}{H}Nz\right)\frac{\sin\left(\frac{\pi}{H}Nz\right)}{\sin\left(\frac{\pi}{H}z\right)}, \tag{11}$$

$D_N(z)$ has the following properties: at $z=0$, $D_N(z)$ achieves its maximum value, while at $z=H$, it reaches its minimum value. Far from these extremes, the amplitude of $D_N(z)$ rapidly diminishes, approaching 0. As $N\to\infty$, $D_N(z)\to\delta(z)$.[19]

Combining Eqs. (9)–(11), we can obtain that $S_0^{[f_1,f_2]}(r,z)$ has four extremums at $z=0$, $z=D$, $z=z_s$, $z=D-z_s$. And the extremums increase as the number of propagating modes N increases, as shown in Fig. 1(a).

Similarly, $S_1^{[f_1,f_2]}(r,z)$ can be expressed as

$$\begin{aligned}S_1^{[f_1,f_2]}(z)&\approx\frac{1}{r}\left[\frac{1}{4}\left(\sum_{n=1}^{N}b_n^{[f_1,f_2]}-\varepsilon_1(z_s)-\varepsilon_1(z)\right.\right.\\&\quad\left.\left.+\frac{\varepsilon_1(z-z_s)+\varepsilon_1(z+z_s)}{2}\right)-G\right],\end{aligned} \tag{12}$$

where

$$\begin{aligned}&\varepsilon_1(z)=\sum_{n=1}^{N}b_n^{[f_1,f_2]}\cos(2k_{zn}z),\\&b_n^{[f_1,f_2]}=\int_{f_1}^{f_2}\frac{|Q(f)|^2}{k_{rn}(f)}\frac{4\rho_0^2}{D^2}\frac{\omega^2}{c^2}\mathrm{d}f.\end{aligned}$$

Similar to $S_0^{[f_1,f_2]}(r,z)$, we can found that $S_1^{[f_1,f_2]}(r,z)$ has four extremums at $z=0$, $z=D$, $z=z_s$, $z=D-z_s$ from Eq. (12), as shown in Fig. 1(b). It should be noted that both $S_0^{[f_1,f_2]}(r,z)$ and $S_1^{[f_1,f_2]}(r,z)$ have maximum values at the source depth. This is because, according to the theory of sound propagation, the peak after the superposition of each order of normal modes is at the depth of the source.[22]

Plugging Eq. (8) into Eq. (7d), we can obtain the following expression of $S_3^{[f_1,f_2]}(r,z)$:

$$S_3^{[f_1,f_2]}(z)\approx\frac{1}{4r}\left[2\varepsilon_3(z)-\varepsilon_3(z+z_s)-\varepsilon_3(z-z_s)\right], \tag{13}$$

where

$$\begin{aligned}&\varepsilon_3(z)=\sum_{n=1}^{N}c_n^{[f_1,f_2]}\sin(2k_{zn}z),\\&c_n^{[f_1,f_2]}=\int_{f_1}^{f_2}|Q(f)|^2\frac{2\rho_0^2}{D^2}k_{zn}\mathrm{d}f.\end{aligned}$$

Using the same method to analyze $S_3^{[f_1,f_2]}(r,z)$, we can find that $S_3^{[f_1,f_2]}(r,z)$ is different from $S_0^{[f_1,f_2]}(r,z)$ and $S_1^{[f_1,f_2]}(r,z)$. At $z=0$ and $z=D$, $S_3^{[f_1,f_2]}(r,0)=S_3^{[f_1,f_2]}(r,D)=0$, and there are two peaks near $z=0$ and $z=D$. At $z=z_s$, $S_3^{[f_1,f_2]}(r,z_s)=0$ and there are two peaks with opposite sign on the left and right sides of the zero point. In the interval between the two peaks, the sign of $S_3^{[f_1,f_2]}$ changes from positive to negative with depth. At mirrored source depth $z=D-z_s$, there is a similar phenomenon.[19] However, the sign of $S_3^{[f_1,f_2]}$ changes from negative to positive in the interval between the two peaks, as shown in Fig. 1(c).

And similar to Eq. (2), we define the normalized broadband Stokes parameters (NBSP) as

$$s_1^{[f_1,f_2]}(z) = \frac{S_1^{[f_1,f_2]}(r,z)}{S_0^{[f_1,f_2]}(r,z)} \approx \frac{\left[\sum_{n=1}^{N} b_n^{[f_1,f_2]} - \varepsilon_1(z_s) - \varepsilon_1(z) + \frac{\varepsilon_1(z-z_s)+\varepsilon_1(z+z_s)}{2}\right] - 4G}{\left[\sum_{n=1}^{N} a_n^{[f_1,f_2]} - \varepsilon_0(z_s) - \varepsilon_0(z) + \frac{\varepsilon_0(z-z_s)+\varepsilon_0(z+z_s)}{2}\right] + 4G}, \tag{14}$$

$$s_3^{[f_1,f_2]}(z) = \frac{S_3^{[f_1,f_2]}(r,z)}{S_0^{[f_1,f_2]}(r,z)} \approx \frac{2\varepsilon_3(z) - \varepsilon_3(z+z_s) - \varepsilon_3(z-z_s)}{\left[\sum_{n=1}^{N} a_n^{[f_1,f_2]} - \varepsilon_0(z_s) - \varepsilon_0(z) + \frac{\varepsilon_0(z-z_s)+\varepsilon_0(z+z_s)}{2}\right] + 4G}. \tag{15}$$

Upon normalization, the range factor is effectively removed. So the NBSP are only related to depths of the source and the receiver, which is the theoretical basis for using Stokes parameters to estimate source depth. And as shown in Fig. 2, the depth distribution law of NBSP is consistent with broadband Stokes parameters. Although the theoretical derivation relies on an ideal waveguide, the conclusions obtained can be generalized to other relatively simple ocean waveguide environments.

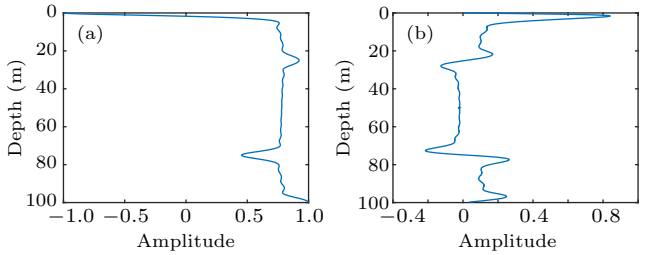


Fig. 2. Evolution of the NBSP in an ideal isovelocity waveguide: (a) $s_1^{[f_1,f_2]}(z)$ and (b) $s_3^{[f_1,f_2]}(z)$.

3. Depth estimation method based on the normalized broadband Stokes parameters

According to Subsection 2.2, we can see that at the depth of the source, $s_1^{[f_1,f_2]}(z)$ has a maximum value. Therefore, we can estimate the source depth by searching the maximum value of $s_1^{[f_1,f_2]}(z)$. For a large aperture vector sensor vertical line array (VSVLA) with M elements, the estimated source depth can be obtained from

$$\hat{z} = \arg\max_{z_j} \left[s_1^{[f_1,f_2]}(z_j) \right], \tag{16}$$

where z_j is the depth of the j-th sensor, where $j = 1$ to M. However, according to our previous work, under the Pekeris waveguide, $s_1^{[f_1,f_2]}(z)$ also exhibits a maximum value at the symmetric depth of the source, which may leads to an erroneous estimation of the source depth. Therefore, we also consider the properties of $s_3^{[f_1,f_2]}(z)$. On both sides of the source depth, $s_3^{[f_1,f_2]}(z)$ has two peaks with opposite signs, located at $z_{\rm pos}$ and $z_{\rm neg}$ ($z_{\rm pos} < z_{\rm neg}$). Within the interval $[z_{\rm pos}, z_{\rm neg}]$, the sign of $s_3^{[f_1,f_2]}(z)$ changes from positive to negative with depth. At the symmetric depth of the sound source, $s_3^{[f_1,f_2]}(z)$ also has two peaks, but between these two peaks, the sign of $s_3^{[f_1,f_2]}(z)$ changes from negative to positive with depth. So we need to determine whether z is within the interval $[z_{\rm pos}, z_{\rm neg}]$. If $\hat{z} \in [z_{\rm pos}, z_{\rm neg}]$, then z is the final estimate for the source depth. Figure 3 shows the flowchart of the algorithm.

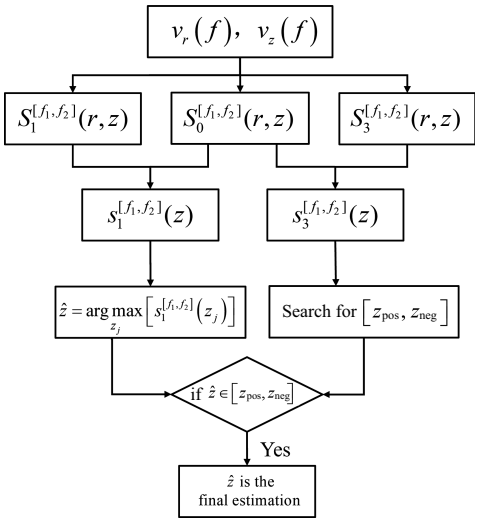


Fig. 3. Flowchart of the proposed method.

The core idea of the proposed approach differs from the traditional MFP in that it is not based on matched processing, leading to differences in estimation capability. The MFP can search for any depth based on the acoustic field model, while the proposed method can only compute $s_1^{[f_1,f_2]}(z)$ and $s_3^{[f_1,f_2]}(z)$ at discrete depths $z = z_j$. In other words, the performance of the proposed method is limited by the depths of the receivers, similar to the data-based MMP.[5] If z_s is not equal to z_j, then this method cannot estimate the true source depth, and the estimation error depends on the minimum of $|z_s - z_j|$. Therefore, when using the proposed method, the array needs to meet two conditions: first, the array aperture covers the depth of the source, and the length of the array is slightly larger than $|z_{\rm pos} - z_{\rm neg}|$; second, the array has a sufficient number of elements to ensure high estimation accuracy. Otherwise, the proposed method may lose its depth estimation capability.

Note that the advantage of the proposed method lies in not requiring environmental information to compute the replica field at different sound source locations. This means that the computational complexity of the proposed method is low and there is no need to consider the impact of environmental information mismatch on estimation accuracy. Since the impact of environmental parameter variations on the Stokes parameter depth distribution at the source depth is small (as analyzed in Subsection 4.1.2), the proposed method exhibits a certain robustness to environmental fluctuations.

4. Simulation and discussion

In this section, we discuss the effectiveness and performance of the proposed method in a simple shallow water waveguide. In the simulation, the KRAKEN software is utilized to compute the particle velocity field. The waveguide simulated in this section is given in Fig. 4. The waveguide has water depth $D = 100$ m with a pressure release seasurface. The seafloor is a semi-infinite basement (constant sound speed $c_b = 2000$ m/s, density $\rho_b = 2000$ kg/m^3, attenuation $\alpha_b = 0.5$ dB/λ). Table 1 provides a list of additional parameters concerning the sound source and array.

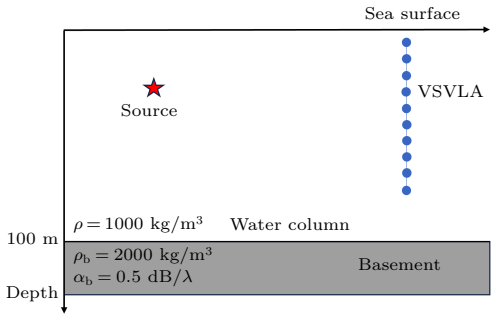


Fig. 4. Simulation environment.

Table 1. Parameters of the source and array.

Parameter	Value
Source depth	25 m
Frequency band	10–250 Hz
SNR	5 dB
Element number	81
Element interval	1 m
Array depth	10–90 m

4.1. Effectiveness

4.1.1. Effect of source depth and range

Firstly, we discuss the influence of source depth and transmission–reception range on the effectiveness of the method. And we established an isovelocity sound speed profile (SSP) ($c = 1500$ m/s). In Fig. 5, $s_1^{[f_1,f_2]}(z)$ and $s_3^{[f_1,f_2]}(z)$ are illustrated across diverse source and receiver depths throughout the entire water column, with a fixed range $r = 5$ km. $s_1^{[f_1,f_2]}(z)$ and $s_3^{[f_1,f_2]}(z)$ change significantly at source depth and mirrored source depth, which aligns with the analysis presented in Section 2 and demonstrates the feasibility of the proposed method for estimating source depth. It can also be observed that regardless of the source depth, extremums of the normalized Stokes parameters exist at the sea surface and seabed. This could impact the results of depth estimation. Therefore, when employing this method, the receiving array should be positioned slightly away from the seabed and sea surface.

Figure 6 shows $s_1^{[f_1,f_2]}(z)$ and $s_3^{[f_1,f_2]}(z)$ for receiver depths spanning the entire water column, range from 3 km to 8 km, with a consistent source depth $z_s = 25$ m. The depth distribution of $s_1^{[f_1,f_2]}(z)$ and $s_3^{[f_1,f_2]}(z)$ is quite similar at each range, because the range terms in the BSP are removed by normalization. This demonstrates the range-independent of the normalized Stokes parameters, indicating that the proposed method is minimally affected by range.

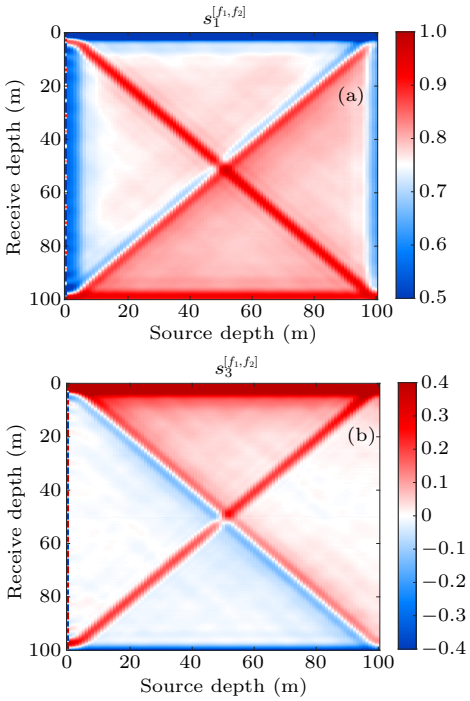


Fig. 5. The NBSP simulated in the ideal isovelocity waveguide with $r = 5$ km: (a) $s_1^{[f_1,f_2]}(z)$, (b) $s_3^{[f_1,f_2]}(z)$.

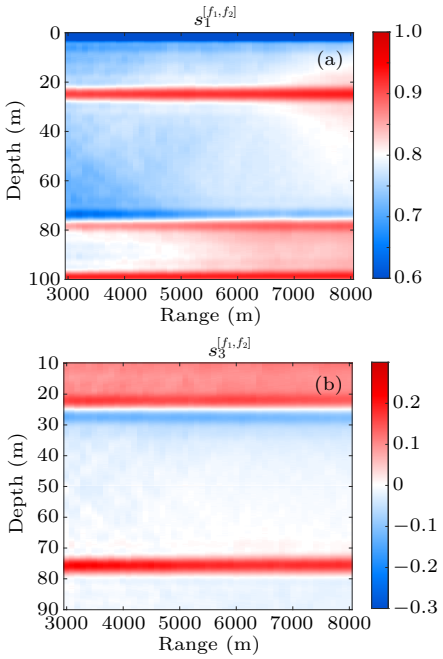


Fig. 6. The NBSP simulated in the ideal isovelocity waveguide with $z_s = 25$ m: (a) $s_1^{[f_1,f_2]}(z)$, (b) $s_3^{[f_1,f_2]}(z)$.

4.1.2. Effect of SSP

Figure 8 shows the NBSP in isovelocity, negative gradient and positive gradient SSPs (as shown in Fig. 7) with $r = 5$ km. From the results, it can be seen that in isovelocity SSP, $s_1^{[f_1,f_2]}(z)$ has 2 peaks located at the source depth $z = 25$ m

and the mirrored source depth $z = 75$ m. The peak located at mirrored source depth interferes with the source depth estimation. So we need to search the sign change interval $[z_{\rm pos}, z_{\rm neg}]$ of $s_3^{[f_1,f_2]}(z)$ to find the correct source depth. Meanwhile, we can observe that the variation in SSP has little impact on the depth distribution law of the Stokes parameters at the source depth. This indicates that the proposed method exhibits robustness to environmental fluctuations.

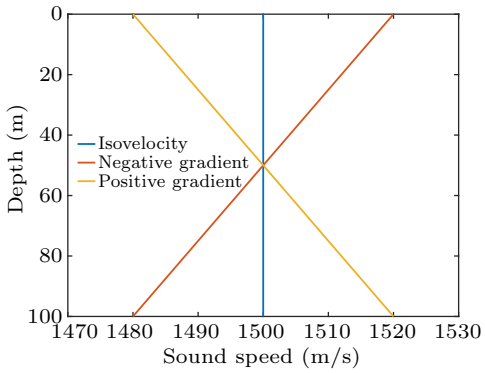


Fig. 7. The three typical shallow-water SSPs.

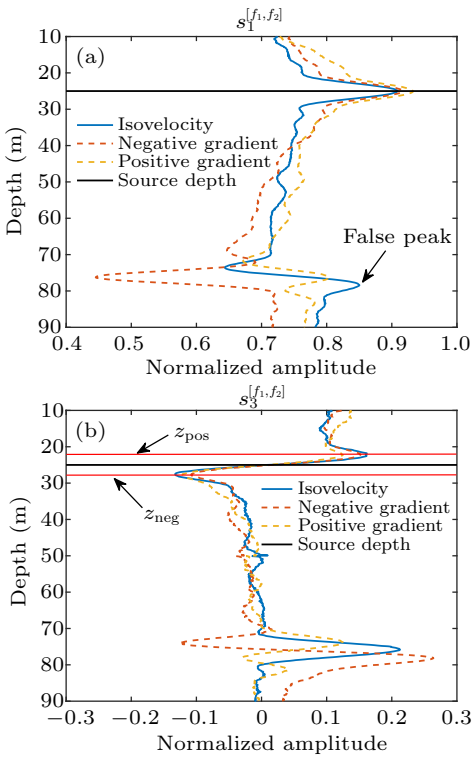


Fig. 8. The NBSP in three shallow-water SSPs: (a) $s_1^{[f_1,f_2]}(z)$, (b) $s_3^{[f_1,f_2]}(z)$.

4.2. Performance evaluation

In this section, we investigate the effects of range, bandwidth and environmental parameters on the performance of the proposed method and compare it with the traditional MFP method. Mean absolute error (MAE) is employed as an evaluation metric for assessing performance

$$\mathrm{MAE} = \frac{1}{L}\sum_{i=1}^{L}|\hat{z}_i - z_{\rm s}|, \tag{17}$$

where $\hat{z}_i$ is the estimated result of the i-th Monte Carlo experiment and L denotes the number of Monte Carlo experiments. The environment parameters of subsequent simulations are illustrated in Fig. 4. In each following section, only one parameter is changed and 100 Monte Carlo experiments are conducted for each scenario.

4.2.1. Range

First, considering the effect of the range between source and receiver, figure 9 shows the evolution of MAE of the proposed method and MFP with source range, range from 4 km to 6 km. For MFP method, the source range in the replica field model is set to 5 km. Parameter mismatch occurs in the MFP method when the actual source range is not 5 km. It can be observed that when the source range is correctly matched, MFP accurately estimates the source depth. However, in cases of source range mismatch, the MAE of the MFP method increases, with a maximum value close to 75 m, indicating that the MFP method is ineffective. For the proposed method, the value of MAE is very small and almost remains constant regardless of range variations, indicating that the performance of the proposed method is minimally affected by range. This is due to the normalized Stokes parameters not containing range-related terms, as can be seen in Section 2. In comparison to MFP, the proposed method is unaffected by range mismatch and demonstrates insensitivity to range.

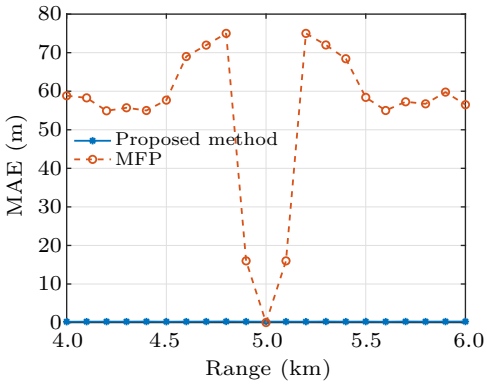


Fig. 9. Variation of the performance with source range.

4.2.2. Bandwidth

The signal bandwidth is a critical parameter of the proposed method. Figure 10 shows the effect of bandwidth, bandwidth from 100 Hz to 500 Hz and band limit $f_1 = 10$ Hz. Evidently, the error of the proposed method decreases as the integrated bandwidth increases. This is because the number of propagating modes N increases, when the upper band limit f_2 increases. More energy of modes is accumulated at the source depth, which increases the peak amplitude and decreases the mainlobe width.[19] The MAE of the MFP method does not vary with the bandwidth because, in cases where the SNR is sufficient, the main factor affecting the accuracy of the MFP estimation is whether the replica field model matches the actual environment.

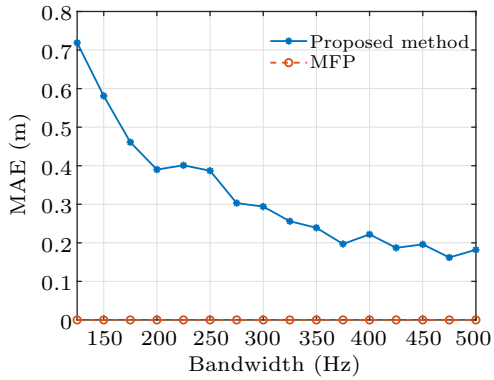


Fig. 10. Variation of the performance with bandwidth.

4.2.3. Environmental parameters

In this section, the effect of environmental parameter is studied. For MFP, the SSP in the replica field model is an isovelocity profile with a sound speed of 1500 m/s. Changes in the sound speed gradient can lead to mismatch in the replica field model. Figure 11 shows the variation of the performance with sound speed gradient. The MAE curve of the proposed method oscillates between 0.3 and 0.4, indicating that the impact of the sound speed gradient on the proposed approach remains relatively minimal. In comparison to the MFP method, it can be observed that when the replica field model and the environment are well-matched, the estimation accuracy of MFP is higher. However, when the replica field model mismatches, the estimation error of MFP increases, and the performance of the proposed method surpasses that of MFP.

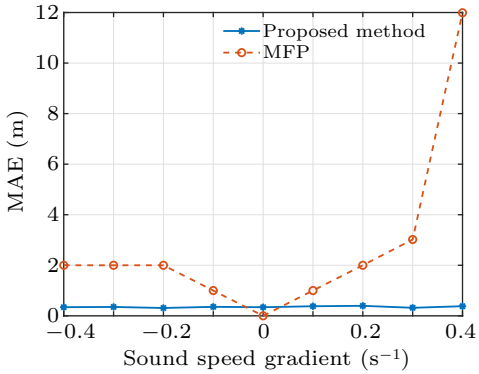


Fig. 11. Variation of the performance with sound speed gradient.

The effect of water depth is given in Fig. 12, water depth from 100 m to 120 m. For MFP, the water depth in the replica field model is set to 100 m. Observing the results, the influence on the proposed approach appears to be inconspicuous. However, for the MFP method, mismatches in water depth have a significant impact on estimation accuracy. When there is a mismatch in water depth, the estimation error of the MFP method is much greater than that of the proposed method, leading to the failure of MFP.

The above results indicate that when the environmental parameters of the replica field model align with the actual environment, the performance of MFP is better; however, when environmental parameters are mismatched, the MFP method is likely to fail. In contrast, the proposed method does not need prior knowledge of environment, eliminating the issue of mismatch. Moreover, variations in environmental parameters have minimal impact on the performance of the proposed method, indicating that the proposed method exhibits good robustness to fluctuations in environmental parameters.

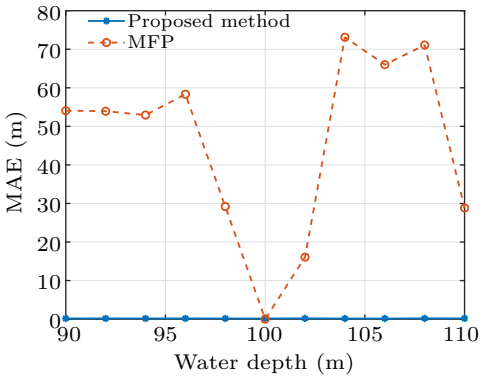


Fig. 12. Variation of the performance with water depth.

4.2.4. SNR

The SNR is a factor that must be considered. The source depth is randomly distributed in 20 m–80 m, the source range is 5 km, SNR from −15 dB to 15 dB. The effect of SNR on MAE is displayed in Fig. 13. The MAE of the proposed method decreases with SNR. The proposed method has good estimation performance when SNR is greater than −5 dB, and the proposed method fails when SNR is less than −5 dB. Compared to the proposed method, under low SNR conditions, MFP still maintains good estimation performance. This is because MFP is an array processing method that can achieve array gain. The proposed method only calculates the Stokes parameters at each array element depth and cannot obtain gain through array processing, thus requiring a higher SNR.

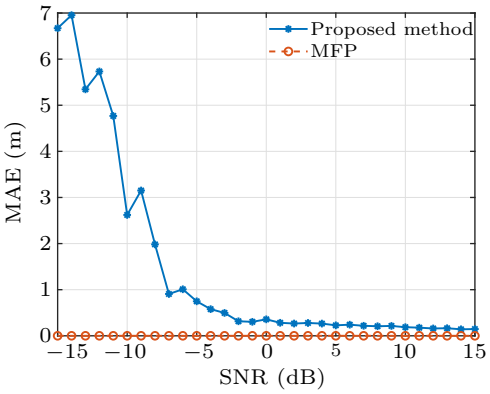


Fig. 13. Evolution of the performance on MAE with SNR.

5. Conclusions

In this paper, the framework of Stokes parameters is used to estimate the acoustic source depth in shallow sea. Through our previous research, we have found that the BSP change significantly at the source depth, and the NBSP are approximately

range-independent. According to these properties, a method is proposed to estimate source depth by extracting the peaks of the NBSP. For precise estimation of the source depth, the array aperture must covers the depth of the source and the array has a sufficient number of elements, which are the limitations of this method. And the advantage of the proposed method is the ability to directly estimate the source depth from received data, without requiring environmental information or considering model mismatch issues. Simulation results have confirmed the efficacy of the proposed method.

After that, the effect of source range, frequency bandwidth, environmental parameters, and SNR on the efficacy of this method is studied and we compared it with the MFP method. It is shown that the proposed method achieves good estimation performance when the SNR is greater than -5 dB. However, it becomes invalid when the SNR is less than -5 dB, while MFP can still accurately estimate the source depth (under matched environmental conditions). But in the case of mismatch in the replica field model, the performance of MFP is worse than that of the proposed approach, and MFP may even fail. However, the proposed method does not need to consider mismatch issues. Furthermore, the performance of the proposed method is minimally affected by environmental parameters, maintaining good estimation performance even when environmental parameters change. This indicates that the proposed method has superior robustness to environmental parameter fluctuations.

It should be noted that the proposed method in this paper is applicable only to single-source scenarios. The method cannot be directly applied to multi-source cases, as interference between multiple sources may alter the characteristics of NBSP, leading to the failure of the proposed approach. However, depth estimation in multi-source environments is of great significance, and addressing this challenging issue will be considered in our future work.

Acknowledgements

Project supported by the National Natural Science Foundation of China (Grant Nos. 12274348 and 12004335) and the National Key Research and Development Program of China (Grant No. 2024YFC2813800).

References

[1] Baggeroer A B, Kuperman W A and Mikhalevsky P N 1993 *IEEE J. Ocean. Eng.* **18** 401
[2] Fawecett J A, Yeremy M L and Chapman N R 1996 *J. Acoust. Soc. Am.* **99** 272
[3] Shang E C 1985 *J. Acoust. Soc. Am.* **77** 1413
[4] Yang T C 1987 *J. Acoust. Soc. Am.* **82** 1736
[5] Yang T C 2014 *J. Acoust. Soc. Am.* **135** 1218
[6] Yang T C and Xu W 2016 *J. Acoust. Soc. Am.* **140** EL302
[7] Zhai D, Zhang B, Li F, Zhang Y and Yang X 2022 *Appl. Acoust.* **192** 108723
[8] Qi Y, Zhou S, Liu C, Dun J and Liu S 2024 *J. Acoust. Soc. Am.* **155** 1103
[9] Liang Y, Chen Y, Meng Z, Zhou X and Zhang Y 2023 *J. Mar. Sci. Eng.* **11** 2059
[10] Qi Y, Zhou S and Liu C 2023 *J. Acoust. Soc. Am.* **154** 2800
[11] Shchurov V A 2011 *Vector acoustics of the ocean* (Beijing: National Defense Industry Press) p. 2 (in Chinese)
[12] Shi C, Zhao R, Long Y, Yang S, Wang Y, Chen H, Ren J and Zhang X 2019 *Natl. Sci. Rev.* **6** 707
[13] Dall'Osto D R and Dahl P H 2013 *J. Acoust. Soc. Am.* **134** 109
[14] Dahl P H and Dall'Osto D R 2020 *IEEE J. Ocean. Eng.* **45** 131
[15] Dahl P H and Dall'Osto D R 2022 *IEEE J. Ocean. Eng.* **47** 680
[16] Bonnel J, Flamant J, Dall'Osto D R, Le Bihan N and Dahl P H 2021 *J. Acoust. Soc. Am.* **150** 1897
[17] Dahl P H and Bonnel J 2022 *J. Acoust. Soc. Am.* **151** 3818
[18] Chen H, Zhu Z and Yang D 2024 *IEEE J. Ocean. Eng.* **49** 1127
[19] Wei Y and Sun C 2024 *J. Mar. Sci. Eng.* **12** 1325
[20] Flamant J and Bonnel J 2023 *J. Acoust. Soc. Am.* **153** 3012
[21] Jensen F B, Kuperman W A, Porter M B and Schmidt H 2017 *Computational Ocean Acoustics*, 2nd edn. (Beijing: National Defense Industry Press) pp. 272–275 (in Chinese)
[22] Zhang H, Xie J, Liu J, Gong L and Li Z 2023 *J. Shanghai Jiaotong Univ.* **58** 995